UC Berkeley
UC Berkeley Previously Published Works

Title

Creation of an axially uniform plasma channel in a laser-assisted capillary discharge

Permalink

https://escholarship.org/uc/item/8fd3468t

Journal

Physics of Plasmas, 28(5)

ISSN

1070-664X

Authors

Bagdasarov, GA
Bobrova, NA
Olkhovskaya, OG
et al.

Publication Date

2021-05-01

DOI

10.1063/5.0046428

Peer reviewed

Creation of an axially uniform plasma channel in a laser-assisted capillary discharge

G. A. Bagdasarov*,[1] N. A. Bobrova,[1] O. G. Olkhovskaya,[1] V. A. Gasilov,[1] C. Benedetti,[2]
S. S. Bulanov,[2] A. J. Gonsalves,[2] C. V. Pieronek,[2, 3] J. van Tilborg,[2] C. G. R. Geddes,[2]
C. B. Schroeder,[2, 3] P. V. Sasorov,[1, 4] S. V. Bulanov,[4, 5] G. Korn,[4] and E. Esarey[2]

[1]*Keldysh Institute of Applied Mathematics, Russian Academy of Sciences, Moscow, 125047, Russia*
[2]*Lawrence Berkeley National Laboratory, Berkeley, California 94720, USA*
[3]*Department of Nuclear Engineering, University of California, Berkeley, CA 94720, USA*
[4]*Institute of Physics ASCR, v.v.i. (FZU), ELI-Beamlines, 182 21 Prague, Czech Republic*
[5]*National Institutes for Quantum and Radiological Science and Technology (QST),*
Kansai Photon Science Institute, Kizugawa, Kyoto, 619-0215, Japan
(Dated: May 25, 2021)

Dissipative capillary discharges form plasma channels which allow for high power laser guiding, enabling efficient electron acceleration in a laser wakefield accelerator. However, at the low plasma densities required to produce high-energy electrons, in order to avoid capillary wall damage, high power lasers need a tighter transverse confinement than cannot be achieved by the capillary discharge powered by Ohmic heating alone. The introduction of an additional laser for heating of the plasma leads to deeper and narrower plasma channels. Here we investigate the formation of laser-heated axially uniform plasma channels. We show that a high degree of longitudinal uniformity can be achieved despite significant evolution of the heater laser during its propagation through the channel.

I. INTRODUCTION

The development of compact, laser-driven plasma acceleration of electrons is one of the most important applications of high intensity short duration lasers [1–3]. One of the advantages of plasma-based accelerators is that they can provide acceleration gradients that are several orders of magnitude higher than those obtained with conventional accelerator technology. Laser wakefield accelerators (LWFAs) have experimentally generated GeV-class electron beams, with the current record energy of 7.8 GeV in a 20 cm plasma [4].

Most laser-plasma acceleration schemes rely on some sort of laser pulse guiding in plasma to extend the acceleration distance. The results reported in Refs. [4, 5] were obtained using capillary discharges operating in the dissipative regime, where the transverse plasma density profile has a minimum on the capillary axis [6, 7]. Such plasma profile ensures guided propagation of laser pulses over distances significantly larger than the Rayleigh length. We note that there are other approaches to creating long plasma channels [8–15].

One of the main drivers behind the development of LWFAs is the possible application of this acceleration scheme to future TeV-scale lepton colliders. It is envisioned that these energies will be reached through staged LWFAs [16], with each stage adding $\sim$10 GeV to the electron beam energy [17]. However, the combined requirements for high laser pulse power and low plasma density lead to possible capillary damage by the wings of the laser pulse. Thus, acceleration of electrons up to $\sim$10 GeV in a single stage becomes problematic for ohmically heated

capillaries as plasma targets. However, the introduction of additional heating of the plasma in a ohmically heated capillary by a ns-duration laser pulse, as suggested in Ref. [18], leads to the deepening of the plasma channel and to the decrease of the matched laser spot size. With this method, a high power laser can accelerate electrons to higher energies due to the reduced plasma density, while being effectively confined to prevent wall damage. The laser heater scheme was successfully demonstrated in Ref. [4] and further studied in Refs. [19, 20]. We note that capillary discharges can operate not only as acceleration modules, but also as transport elements for charged particle beams [16, 21–27]. In what follows we report on the theoretical and computer simulation studies of the laser heating of capillary discharges in order to optimize the plasma target for LWFA applications.

The laser heating scheme, as introduced in Ref. [18], was based on the 1D model, which employed 1 ns laser pulse with matched to the channel spot size and assumed longitudinal homogeneity of the interaction. Subsequent experimental and computer simulation studies [4, 19, 20] revealed that 3D effects play an important role, significantly modifying the interaction. While $\sim$1 ns laser pulses produced strongly oscillating, both in terms of depth and matched spot size, plasma channels, $\sim$10 ns pulses formed quasi-stable channels suitable for LWFA operation.

The results of Refs. [4, 19, 20] demonstrated a set of parameters for which a sufficiently axially uniform plasma channel is obtained. Nevertheless, the mechanism yielding to the creation of such longitudinally uniform plasma taking place after a nonuniform transient stage, was not understood. The simulations of the capillary plasma dynamics modified by the laser heater [4, 19, 20] were performed using the multi-dimensional code MHD solver from the MARPLE framework [28] coupled with additional modules from INF&RNO [29, 30], which added

---

the capability to calculate the heater laser pulse propagation. In this paper we detail the coupling of MARPLE and INF&RNO codes as well as the plasma dynamics under the action of the laser heater.

In what follows we report on the results of the study of the plasma density evolution in the capillary, and, in particular, the source of the plasma channel axial uniformity after the passage of the laser heater. We show that this axial density homogenization is due to the transverse relaxation and not to the longitudinal dynamics.

The electron density distribution in the capillary discharge, which is modified by the laser heater, depends on a number of parameters: capillary diameter and length, initial gas density and species, peak electric current, the duration of the current pulse, wavelength, duration, spot size, and the total energy of the laser heater and high power laser pulse. Though it is challenging to study this vast parameter space, the values of some parameters can be fixed due to the availability of specific laser systems. In this work we study three main parameters: the duration of the heater pulse, τ_ℓ; the delay between the electric current peak, $T/2$, and the heater pulse, t_0; and the delay between the heater pulse and the high power laser pulse, $t - t_0$. Here we assume $\tau_\ell = 8$ ns for the simulations.

The paper is organized as follows. Sec. II is devoted to the two-dimensional plasma simulations. We describe the physical model, the coupling of the MARPLE and INF&RNO codes, the initial and boundary conditions, and the results of the simulations. The mechanism yielding to the axial uniformity of the electron density distribution is investigated in Sec. III. Conclusions are presented in Sec. IV.

II. 2D MHD SIMULATIONS

A. Physical model

The plasma density distribution evolution of a laser-heated capillary discharge is determined by the two processes: the discharge plasma dynamics, and the laser pulse dynamics in the underdense plasma. The first one is described by a one-fluid, two-temperatures magnetohydrodynamic (MHD) approximation, where magnetic field diffusion, electron and ion thermal conductivities, Joule heating, and radiation losses are taken into account [6]. The system of equations used to model the capillary discharge dynamics reads as follows [31]:

$$\partial_t \rho + \nabla(\rho \mathbf{v}) = 0, \tag{1}$$

$$\rho(\partial_t + \mathbf{v}\cdot\nabla)\mathbf{v} = -\nabla p + \mathbf{j}\times\mathbf{B}/c, \tag{2}$$

$$\rho(\partial_t + \mathbf{v}\cdot\nabla)\varepsilon_i + p_i\nabla\mathbf{v} = \nabla(\kappa_i\cdot\nabla T_i) + Q_{ei}, \tag{3}$$

$$\rho(\partial_t + \mathbf{v}\cdot\nabla)\varepsilon_e + p_e\nabla\mathbf{v} =$$
$$= \nabla(\kappa_e\cdot\nabla T_e) - Q_{ei} + Q_{rad} + \mathbf{j}^2/\sigma + Q_l, \tag{4}$$

$$\partial_t\mathbf{B} + \nabla\times(\nu_m\cdot\nabla\times\mathbf{B}) = \nabla\times(\mathbf{v}\times\mathbf{B}), \tag{5}$$

$$\mathbf{j} = c/4\pi\cdot\nabla\times\mathbf{B}, \quad \nu_m = c^2/4\pi\sigma. \tag{6}$$

Here ρ is the plasma density; $p = p_i + p_e$ is the plasma pressure, which is the sum of the electron and ion pressures; $\mathbf{v}$ is the plasma velocity; $\mathbf{B}$ is the magnetic field; ε_e and ε_i are the internal energies of the electron and ion components, respectively, per unit of plasma mass; Q_{ei} is the rate of the thermal transfer between electrons and ions (neutrals); Q_{rad} is radiation losses; T_e and T_i are the electron and ion temperatures, respectively; $\mathbf{j}$ is the electric current density, σ is the electric conductivity; κ_e, κ_i are the thermal conductivities of electrons and ions, respectively, and Q_l is the energy deposition from the laser pulse to the plasma electrons (see below). We used this model (excluding the Q_l term) for 2D/3D simulations of dissipative discharges [32–34] and it proved to be qualitatively and quantitatively accurate.

The discharge dynamics are investigated in a capillary pre-filled by non-ionized hydrogen. The properties of the hydrogen plasma were described in Ref. [6]. The model assumes local thermodynamic equilibrium for ionization degree of moderate and fully ionized hydrogen plasma. The energy cost due to the ionization is included in the specific energy of electrons, ε_e. The degree of ionization determines p_e and ε_e. The electric conductivity σ as well as the electron thermal conductivity κ_e are determined by the collisions of electrons with both ions and neutrals.

The laser pulse evolution is described through the solution of the paraxial wave equation [2], where we assume that the laser pulse has a moderate amplitude, $\hat{a}(x, y, z, t)$, which is a smooth function of time and space, and propagates along the z-axis:

$$\nabla_\perp^2\hat{a} + 2ik_0(c^{-1}\partial_t\hat{a} + \partial_z\hat{a}) = 4\pi r_e n_e\hat{a}. \tag{7}$$

Here, n_e is the electron density, $r_e = 2.8179\cdot10^{-13}$ cm is the classical electron radius. The transverse component of the electric field in the electromagnetic wave is defined as $E(x, y, z, t) = \hat{a}(x, y, z, t)\exp(ik_0z - i\omega t)/2 + $ c.c., $\omega = k_0 c$, $k_0 = 2\pi/\lambda$, and λ is the laser wavelength. The equation corresponds to the well-known classic Helmholtz paraxial approximation, accounting for a small departure of the plasma refractive index from unity.

The MHD and laser propagation equations are coupled through the energy deposition, Q_l, which determines how the laser energy is transferred to the plasma, and the electron density, n_e, which determines the laser evolution. The value of Q_l is determined by the inverse bremsstrahlung absorption. The following formulae are used to evaluate the energy deposition from the laser pulse to the plasma:

$$Q_l = \frac{|E|^2}{8\pi}\omega\varepsilon''(n_e, T_e, z), \tag{8}$$

$$\varepsilon'' = \frac{4\sqrt{2\pi}}{3}\cdot\frac{q_e^4 n_e}{\sqrt{m_e T_e^3}}\cdot\frac{\omega_{pe}^2}{\omega^3}\Lambda, \tag{9}$$

$$\Lambda = \max\left[\frac{\pi}{\sqrt{3}}, \frac{1}{2}\ln\left(\frac{2^5\cdot T_e^3}{e^{5\gamma}\cdot\omega^2 q_e^4 m_e}\right)\right], \tag{10}$$

where ε'' is the imaginary part of the dielectric constant: $\varepsilon = \varepsilon' + i\varepsilon''$, $\gamma = 0.57721\ldots$ is Euler-Mascheroni

constant, ω_{pe} is the plasma frequency, q_e and m_e are the electron charge and mass, respectively. These expressions for the rate of hydrogen plasma heating due to the absorption of the laser pulse energy via the inverse bremsstrahlung process are valid when $\hbar\omega \ll T_e \ll q_e^4 m_e/\hbar^2 \sim 27\,\mathrm{eV}$ and $\omega \gg \omega_{pe}$ [35, 36].

B. Computer code integration

The MHD solver from the MARPLE framework [28] is used for the simulations of the capillary discharge plasma dynamics. The INF&RNO code [30] is used to model the laser pulse propagation through the underdense plasma. MARPLE implements the MHD model (1)-(6). A subset of the INF&RNO routines to solve equation (7) was incorporated into the MARPLE framework together with (8)-(10) in order to self-consistently model the laser heating of the capillary discharge plasma.

The codes use different geometrical, numerical, and computational approaches to solve the corresponding equations. MARPLE's MHD solver is a 3D Eulerian "parallel" code, while INF&RNO is a 2D cylindrical serial code with co-moving coordinates. These differences were taken into account to achieve consistent operations of both codes without any essential modifications. The final code provides accurate modeling of laser-assisted capillary discharge plasma dynamics in (r, z) geometry.
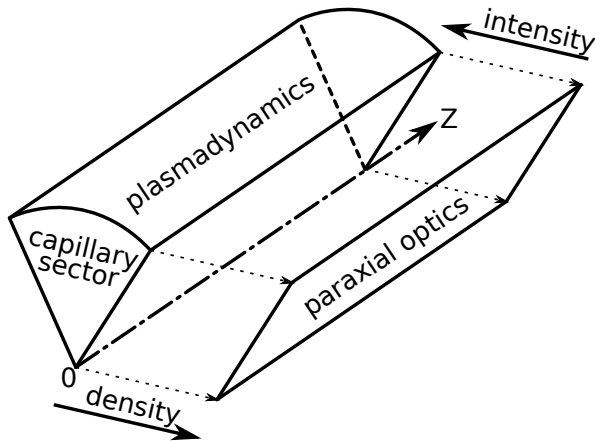

FIG. 1: Conceptual approach towards computer simulations of the laser-assisted capillary discharge.

The combined code operation is schematically shown in Fig. 1. A cylindrical sector represents a capillary and is used as a computational domain for the MHD solver, while only one of its side faces is used for INF&RNO calculations. The combined code performs calculations sequentially in a loop. The loop starts with the calculation of the laser pulse propagation. First, the electron density distribution from the MHD solver is input in the the INF&RNO routines to advance the laser propagation. The values from the one face of the cylinder sector are used here, because the discharge is assumed to be axisymmetric. The resulting laser intensity distribution is then input in the MHD solver and used to calculate the energy deposition. The loop ends with the discharge plasma dynamics calculations, taking into account the additional energy deposition. This procedure is repeated until the laser heating is finished. Before the beginning of the heater pulse and after its end, the loop is simplified to the discharge simulation only.

The combined code provides results that are in good agreement with the experiments, as shown in Refs. [4, 19, 20]. Note that the described code can model only azimuthally symmetric problems. We can simulate only circular cross-section capillaries, and cannot take into account influence of open ends and supply channels, as well as imperfect non-symmetric focusing of the heater laser pulse.

C. Simulation setup

The cylindrical 60-degrees sector with periodic boundary conditions on its radius side was used to represent a 20 cm-long capillary with $800\,\mu\mathrm{m}$ diameter, see Fig. 1. Initially the capillary is filled uniformly with non-ionized hydrogen (effective charge $Z \ll 1$) with density $\rho = 10^{-6}\,\mathrm{g/cm^3}$, and temperatures $T_e = T_i = 0.5\,\mathrm{eV}$ of electrons and ions, respectively. The magnetic field B_φ corresponding to the sinusoidal discharge current $I(t) = I_0 \cdot \sin(\pi t/T)$ with maximum $I_0 = 450\,\mathrm{A}$ and period $T = 800\,\mathrm{ns}$ is set on the outer face of the cylindrical sector. A laser heater pulse, centered at time $t = t_0$, with Gaussian temporal and transverse profiles is set on the $z = 0$ boundary. Its total energy is 300 mJ, the wavelength $\lambda = 532\,\mathrm{nm}$, the FWHM duration $t_w = 8\,\mathrm{ns}$ and the focused spot size $w_0 = 84\,\mu\mathrm{m}$. The delays from 0 to 400 ns between the peaks of the electric current and the laser pulse were investigated in the simulations. The discharge plasma dynamics is simulated in the interval from 0 to 1000 ns taking into account active laser heating during $[t_0 - 1.5\,t_w,\ t_0 + 2.5\,t_w]\,\mathrm{ns}$. The delay $t_0 - T/2$ is set to be $(0, 100, 200, 300, 400)\,\mathrm{ns}$.

D. Simulation results

As the electric current flows through the capillary, it heats and ionizes the hydrogen gas, generating plasma which forms an approximately parabolic channel with the density minimum at the capillary axis due to the cooling at the capillary wall. The evolution of the plasma density and temperature are shown in Fig. 2. Approximately after 200 ns of the discharge, a quasi-steady plasma channel is formed. Its parameters depend only on the initial gas density, discharge current, and capillary radius [6].

The laser heater is introduced when the capillary discharge is in the quasi-steady state. As the laser heater propagates through the channel, it heats the plasma near the capillary axis, which leads to the deepening of the

plasma channel, see Fig. 3. This deepening is shown in detail in Fig. 4, where one can see the evolution of the plasma density and temperature at the central capillary axis at $z = 0$ for different delays between the maximums of the current pulse and the laser heater. We note that for longer delays, which correspond to lower values of plasma temperature a deeper channel is produced.
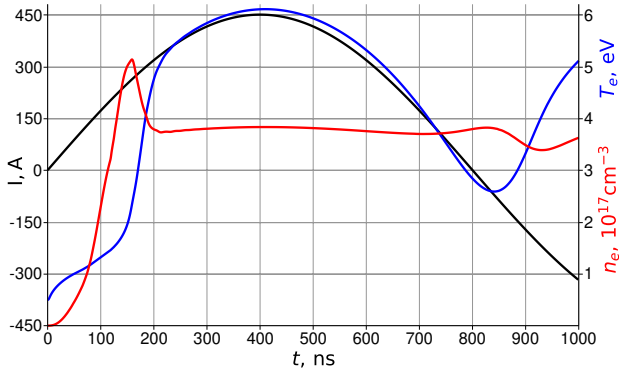

FIG. 2: Time evolution of the electric current (black), the electron density (red) and temperature (blue) on the capillary axis in the discharge without additional laser heating.
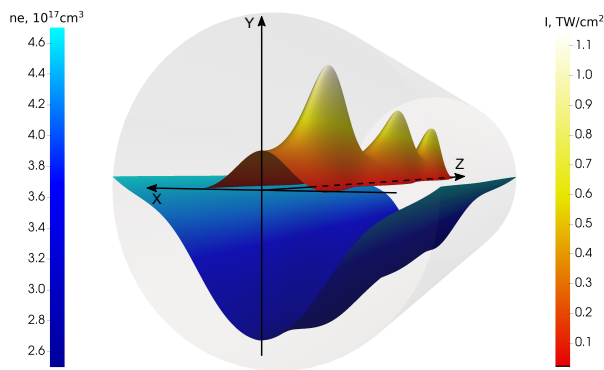
FIG. 3: Electron density (blue palette) and laser heater intensity (red palette) distributions at $t = t_0 = 800$ ns.

According to Fig. 4, the modification of plasma density happens on time scales shorter than the laser heater duration. Hence, if the head of the pulse was matched to the plasma channel, the tail will be mismatched. This will lead to the modulation of the laser heater transverse size, $w(z, t)$, and, thus, of its intensity, see Fig. 5. Therefore, the amount of heating each plasma element receives depends on its position and time.

The electron density profile of the modified channel is also modulated, see Fig. 6. During the time interval $t_0 - 0.5\, t_w < t < t_0 + 1.5\, t_w$ both heater pulse and plasma channel have essentially modulated axial profiles with maximum variation around $t - t_0 = 0$, when the laser heater intensity reaches its maximum. While for later times, $t - t_0 \geq 1.5\, t_w$, they become almost uniform, i.e. the maximum variation of the axial electron density
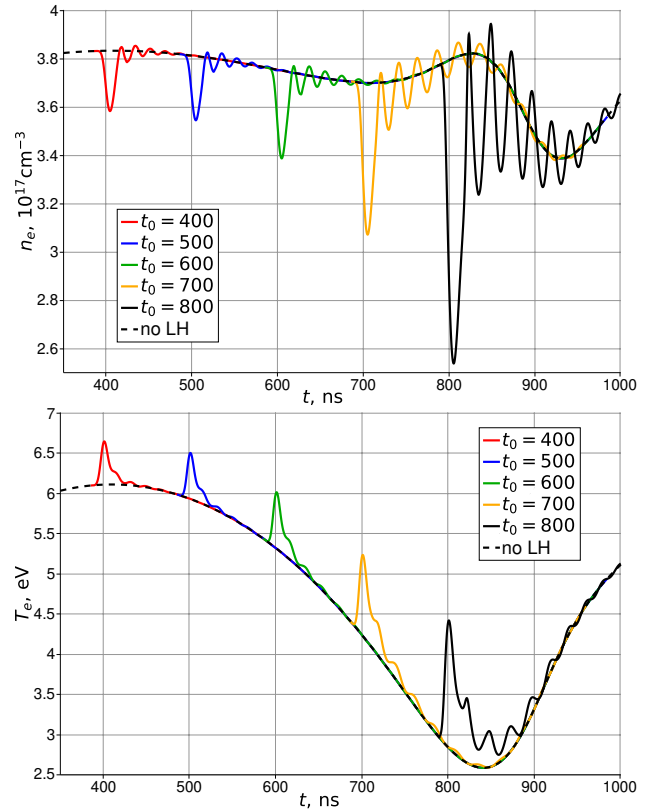

FIG. 4: Time evolution of electron density (top) and temperature (bottom) at the capillary axis ($z = 0$) for different delays between the maxima of electric current and laser heater.

is less than 3% for any time in $t - t_0 \in [1.5\, t_w,\ 2.5\, t_w]$. Such degree of longitudinal uniformity is observed for each delay, $t_0 - T/2$, considered in this work. The same property is observed for a top hat transverse heater profile, see Refs. [19, 20]. The aligning effect is discussed in details in Sec. III.

In order to evaluate the uniformity of the modified plasma channel we also need to analyze its radial profile. The dissipative discharge in a circular cross-section shape capillary produces a parabolic channel profile given by $n_e(r)/n_e(0) = 1 + a(r/R)^2$, where R is the channel radius [6]. The additional heating produces a parabolic a sub-channel atop of the main channel, as can be expected from the symmetry of the problem. This is observed in the simulations, see Fig. 3. Thus, the coefficient $a = a(z, t)$, determined by the electron density profile at $r \leq 200\, \mu$m, is a suitable parameter to analyze the radial profile of the sub-channel, see Fig. 7. Its evolution looks similar to the evolution of the channel's axial electron density (Fig. 6). Modulations of the parameter a are present in the interval $t_0 - 10 < t < t_0 + 20$ ns, when the laser heating occurs, and are rather weak after the heating pulse leaves the capillary.

The purpose of the additional laser heating of the capillary discharge plasma is to deepen the original plasma channel as much as possible, while maintaining unifor-
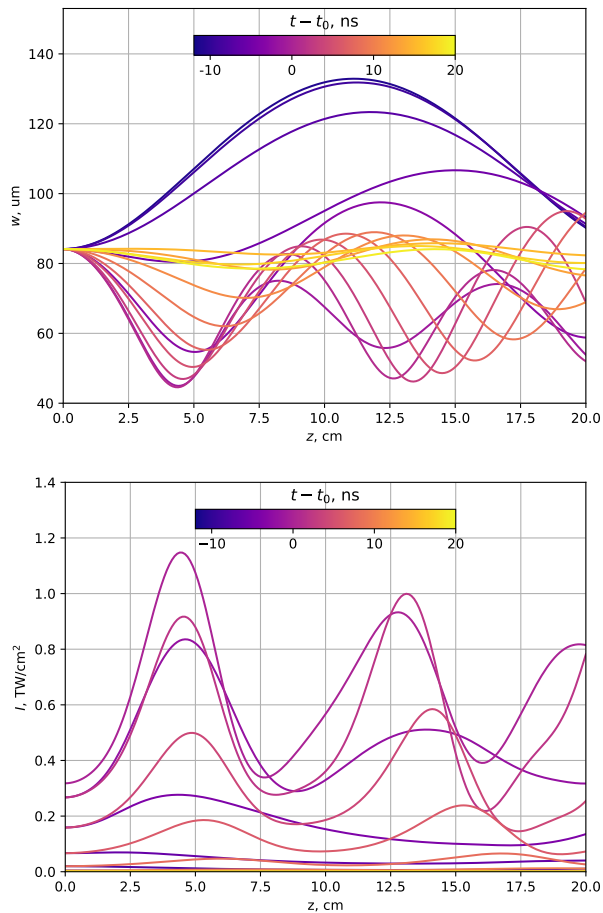
FIG. 5: Axial distributions of heating laser pulse transverse size $w(z, t)$ (top) and its axial intensity (bottom) for time interval $t_0 - 10 < t < t_0 + 20$ ns, $t_0 = 800$ ns.
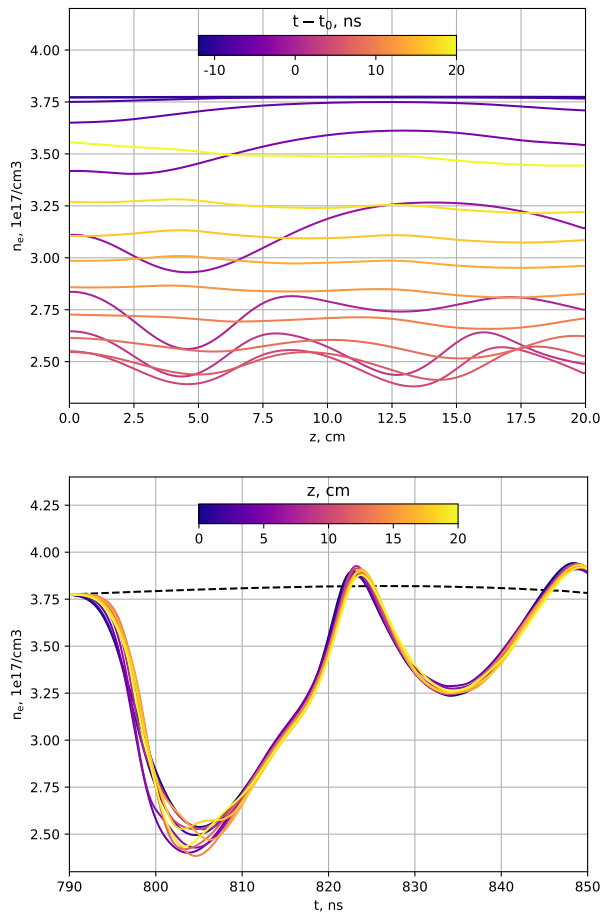

FIG. 6: Axial electron density $n_e(r = 0, z)$ dynamics during heating pulse propagation for time interval $t_0 - 10 < t < t_0 + 20$ ns, $t_0 = 800$ ns.

mity in the longitudinal direction. Both of these requirements can be satisfied by operating at the maximum of the following function

$$f(t, t_0) = \frac{\frac{\Delta n_e}{\bar{n}_e}}{\sqrt{\left(\frac{\sigma_{n_e}}{\bar{n}_e}\right)^2 + \left(\frac{\sigma_a}{\bar{a}}\right)^2}} . \qquad (11)$$

Here σ_{n_e} is a standard deviation of the instantaneous axial distribution of $n_e(x = y = 0, z, t)$ around its mean value $\bar{n}_e$ at the same time:

$$\sigma_{n_e}^2(t) = \frac{1}{L_z} \int_0^{L_z} [n_e(x = y = 0, z, t) - \bar{n}_e(t)]^2 \, dz;$$

$$\bar{n}_e(t) = \frac{1}{L_z} \int_0^{L_z} n_e(x = y = 0, z, t) \, dz \, ;$$

σ_a and $\bar{a}$ are defined analogously for the parameter $a(z, t)$; Δn_e is defined as the difference between the values of $\bar{n}_e$ calculated with and without the heater; and L_z

is the length of the capillary. The parameter $f(t, t_0)$ characterizes the effectiveness and quality of the laser heater action. It depends on two parameters: the time delay $t - t_0$ between the heater maximum and the peak of the high-power main pulse; and the time delay $t_0 - T/2$ between the maximum of the electric current pulse through the capillary and the peak of the heater. The most effective heating corresponds to the maximum of the function f.

The time interval where the maximum of f should be searched is bounded by the times when the axial density distribution reaches its first two extrema, see Fig. 6. Dependencies of $f(t, t_0)$ on t for several values of t_0 are shown in Fig. 8. Optimal parameters for the electron density distributions as a function of t_0, determined by the maximum of $f(t, t_0)$, are summarized in Tab. I. We note that in the case of an optimization of a LWFA with a non-matched high intensity pulse, the function f should be cast in a different form, taking into account the nonlinear evolution of the spot size of the high intensity pulse. Such study lies beyond the scope of this paper.
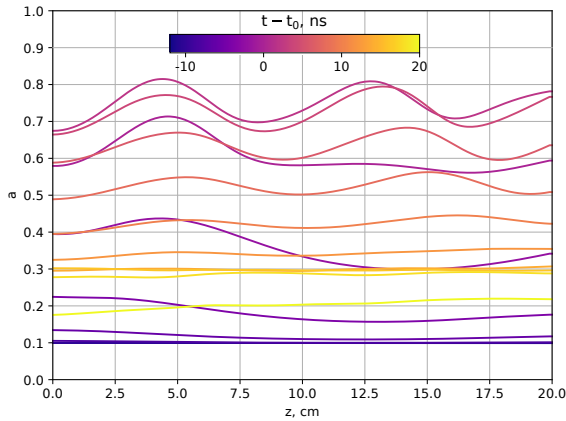
FIG. 7: Evolution of coefficient a, defined by $n_e(r)/n_0 = 1 + a(r/R)^2$, where $0 \le r \le R = 200\,\text{nm}$, for time interval $t_0 - 10 < t < t_0 + 20\,\text{ns}$, $t_0 = 800\,\text{ns}$.
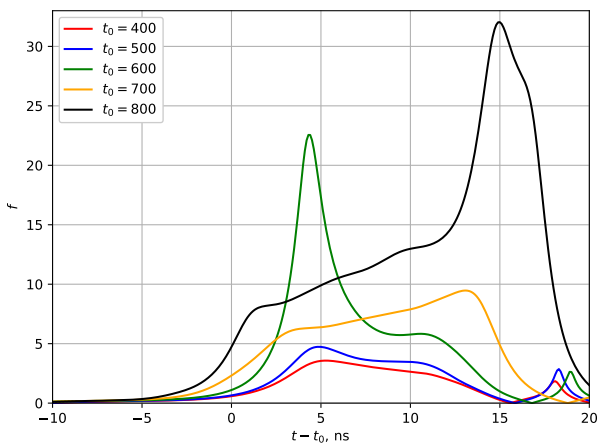

FIG. 8: Dependence of function $f(t, t_0)$ on $t - t_0$ for several values of t_0.

III. MECHANISM FOR THE AXIAL ALIGNING OF THE ELECTRON DENSITY DISTRIBUTION

In this section we discuss why the laser heating of the capillary discharge plasma leads to the formation of an approximately longitudinally homogeneous channel after the laser heater. This phenomenon is particularly interesting since the heating of the plasma leads to significant modulation of the transverse size of the laser heater as it propagates through the capillary (see Figs. 5 and 6), which is due to the variation of the matched spot size for single mode propagation along the pulse. One could expect this variation to lead to completely different heating of different slices of the capillary and, thus, to a modified channel with large variations of the on-axis density and width of the channel. However, simulation results reported in the previous section show that the formation of a longitudinally homogeneous plasma channel is possible, see Figs. 6, 7 and 9.

TABLE I: Optimal channel parameters, times of their formation and the maximums of function f.

t_0	ns	400	500	600	700	800
$t - t_0$	ns	5.3	4.9	4.3	13.1	15.0
$10 \cdot a$		0.85	0.88	0.97	1.01	0.91
$10 \cdot \overline{a}$		1.45	1.59	2.09	1.82	2.95
n_e	$10^{17}\,\text{cm}^{-3}$	3.83	3.81	3.75	3.70	3.81
$\overline{n_e}$	$10^{17}\,\text{cm}^{-3}$	3.60	3.56	3.39	3.38	3.04
f		3.58	4.74	22.56	9.47	32.04

We note that there is no apparent physical mechanism for relaxation of the plasma parameters along the 20 cm long capillary. Thus, the transverse plasma dynamics in the channel should be responsible for this relaxation. Since the capillary is cylindrical, this is a one-dimensional effect. In principle, from the analysis of the initial conditions and the interaction setup one can draw a conclusion about the dominance of the transverse plasma dynamics. The key parameters determining the evolution of the heated capillary discharge such as capillary radius, initial hydrogen gas density distribution, electric current flux, and total energy flux of the laser heater do not depend on the longitudinal coordinate. The latter statement implies that the laser heater depletion is negligible.

If these conclusions are true, then the complex evolution of the transverse size of the laser beam, $w(z, t)$, does not significantly affect the plasma density profile formed in the wake of the laser heater. The results of the MHD simulations are in good agreement with these conclusions, see Fig. 9. In what follows we show that 1D MHD simulations of the transverse plasma dynamics give almost the same result for the plasma density distribution.

Let us consider the characteristic transverse and longitudinal plasma relaxation times. They depend on the duration of the current pulse, τ_e ($\sim$500 ns), and the laser heater, τ_l ($\sim$8 ns), capillary length, L_z (20 cm), capillary radius, R_0 (400 μm), and the width of the laser heater, w_0 ($\sim$80 μm). The rate of the plasma relaxation depends on the following parameters: typical sound velocity, c_s, the coefficient of plasma temperature diffusion, χ, and magnetic viscosity, v_m. The latter determines the rate of the electric current diffusive redistribution over the capillary cross section. The sound velocity can be evaluated as $c_s = \sqrt{2T_e/Am_a}$, where T_e is the temperature of the fully ionized hydrogen plasma, 3–6 eV in our case, $A = 1$ for hydrogen, and $m_a = 1.6605 \cdot 10^{-24}$ g is the atomic mass unit. Thus, typical sound velocity can be estimated as $c_s = 3 \cdot 10^6$ cm/s. The temperature diffusion coefficient is defined as $\chi = \kappa_e/C_v$, where κ_e is coefficient of electron thermal conductivity, and $C_v = 3n_e$ is plasma volume heat capacity. For typical electron temperature and density, $n_e \sim 3 \cdot 10^{17}$ cm^{-3}, we evaluate $\chi \sim (2$–$9)\cdot 10^4$ cm^2/s. The magnetic viscosity is estimated as $\nu_m \sim (1.5$–$3)\cdot 10^5$ cm^2/s for the same conditions.

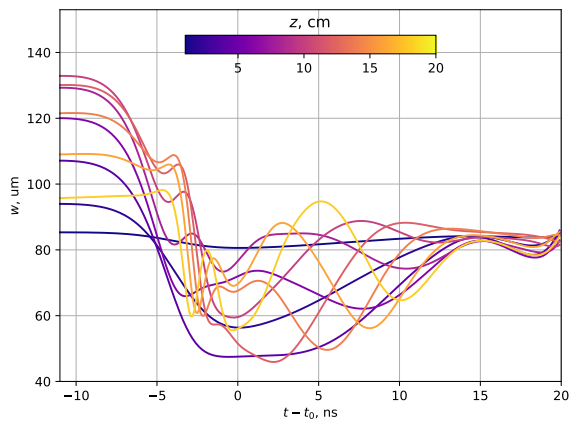Using the above definitions we estimate the typical

FIG. 9: Matched spot size, $w(z,t)$, simulated with MARPLE+INF&RNO, versus $t - t_0$ at several axial positions, z. $t_0 = 800$ ns.

scale of plasma relaxation in longitudinal and transverse dimensions of the capillary discharge when only the electric current is present: $c_s \tau_e \sim 1$ cm and $\chi \tau_e \sim (1-5) \cdot 10^{-2}$ cm^2. Comparing the length and radius of the capillary yields

$$c_s \tau_e \ll L_z, \qquad \chi \tau_e \ll L_z^2, \qquad (12)$$

$$c_s \tau_e \gg R_0, \qquad \chi \tau_e \gg R_0^2. \qquad (13)$$

It follows from Eq. (12) that neither pressure, nor temperature relaxation in the longitudinal direction are efficient on the time scale τ_e, determined by the electric current pulse. Thus, the axial uniformity of the capillary discharge without laser heating should be provided by the capillary geometry, and initial and boundary conditions uniform in the z direction. We note that these considerations are no longer valid near the capillary exits. Since the plasma density distribution at the exits is affected by the open space outside the capillary with the characteristic length of the affected region of the order of 1 cm, as was shown in Ref. [32]. In contrast to the longitudinal direction, the transverse one (13) demonstrates opposite behavior, i.e., the plasma dynamics is determined by the relaxation. That is why the quasi equilibrium model [6] is applicable for the description of the capillary plasma discharge. The model implies that the plasma is in dynamic and thermal quasi-equilibrium in each cross section of the discharge.

If we consider the typical scale of plasma relaxation in the capillary discharge during the action of the laser heater, then for the longitudinal dimension we obtain the following relations

$$c_s \tau_l \ll L_z, \qquad \chi \tau_l \ll L_z^2, \qquad (14)$$

which show that neither pressure, nor temperature relaxation in the axial direction are efficient during the laser heater propagation. However, in the transverse direction the situation is different, with

$$c_s \tau_l \sim R_0, \qquad \chi \tau_l \sim R_0^2. \qquad (15)$$

Hence, the transverse dynamics of the capillary plasma under the action of the laser heater is significantly non-stationary. However, if we consider the plasma dynamics inside the laser heater,

$$c_s \tau_\ell > w, \qquad \chi \tau_\ell > w^2, \qquad (16)$$

we can conclude that the plasma relaxation plays an important role in the evolution of the plasma density profile near the central axis of the capillary. Moreover, we can assume that the change of the laser beam transverse size is not so important once the total energy flux in the beam does not depend on z. This assumption is confirmed by the set of the one-dimensional (r,t)-simulations of the capillary plasma dynamics.

In what follows we employ the 1D code NPINCH, previously used to simulate different types of capillary discharges (see for example Refs. [6, 37, 38]). We note that the agreement between MARPLE and NPINCH codes is good at the level of 3–6%, see e.g. Ref. [32].

The 1D physical model used in the code NPINCH does not consider heater laser beam propagation along the z-axis. It corresponds just to one cross section of the capillary discharge at a single value of z, implying that z-dependencies of all variables are smooth enough. The energy flux $F(r,t)$ of the heater laser (measured for example in erg/cm^2/s) is

$$F(r,t) = \frac{|E|^2}{8\pi} c = \frac{4\sqrt{\ln 2}}{\pi^{3/2}} \frac{\mathcal{E}_\ell}{w^2(t)\tau_\ell}$$
$$\times \exp\left[-2\frac{r^2}{w^2(t)} - \frac{(t-t_0)^2}{\tau_\ell^2} 4\ln 2\right], \quad (17)$$

where $\mathcal{E}_\ell$ is the total energy of the heater pulse, $w(t)$ is the radius of the beam (at $1/e^2$-level of its maximum at the axis), τ_ℓ is the duration of the pulse (that is its full width at half maximum), and t_0 is the moment of laser pulse maximum. The laser pulse propagating through the capillary plasma leads to its heating in accordance with expressions (8)-(10). The laser wavelength λ, $\mathcal{E}_\ell$, τ_ℓ and the set of t_0 are the same as in the 2D simulations, presented in Sec. II. The electric current profile, the diameter of the capillary, as well as the initial hydrogen density are also the same.

The main goal of the 1D simulations is to show that at some moment in time t, $t - t_0 \gtrsim \tau_\ell$, the radial distribution of the electron density is almost independent of the value of $w(t)$. In order to illustrate this we set $w(t) = \text{constant} = w_0$, and choose a discrete set of the w_0 values: $w_0 = 60$, 90 and 120 μm for $t_0 = 800$ ns.

The evolution of the axial values of n_e and T_e during the time period $t - t_0 \in (-12, 38)$ ns for the three values of w_0 is shown in Fig. 10. The differences between the
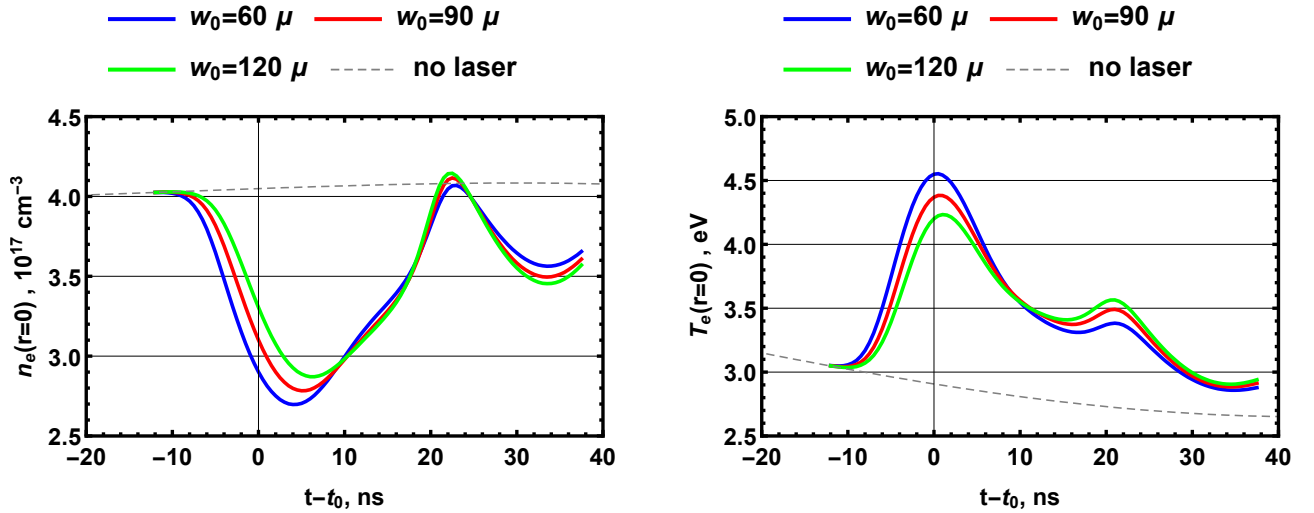
FIG. 10: Time evolution of axial electron density $n_e(0, t)$ (left frame) and temperature $T_e(0, t)$ (right frame), obtained in 1D simulations with code NPINCH during the heater laser pulse and after for $t_0 = 800$ ns and $w_0 = 60$, 90 and 120 ns.
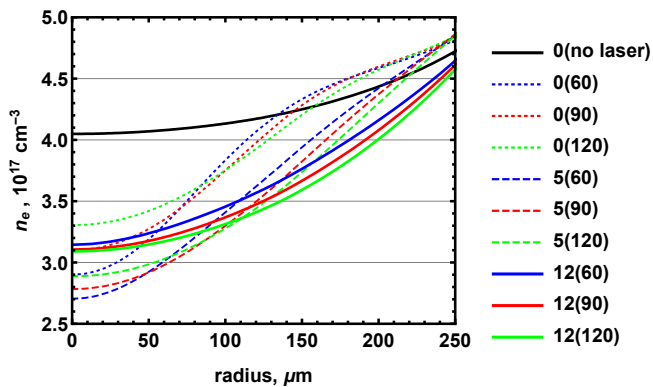

FIG. 11: The radial electron density profiles in the vicinity of the capillary axis for different $w_0 = 60$, 90 and 120 μm, $t_0 = 800$ ns and $t - t_0 = 0$, 5 and 12 ns. The curves are labeled by $\delta\tau(w_0)$, where $\delta\tau = t - t_0$ in ns, and w_0 in μm.

FIG. 12: The comparison of plasma parameters radial profiles at $t - t_0 = 12$ ns and $t_0 = 800$ ns with the heater laser ($w_0 = 60$ μm) and without it. The dashed lines show electron temperature profiles, and solid lines show electron density profiles. The black lines show the case without heater and the red lines show the case with the heater. We see that size of deformation of plasma parameters profiles (~ 250 μm) is considerably larger than the laser heater size (~ 60 μm).

curves corresponding to different w_0 values reach their maxima in the vicinity of the laser pulse maximum. After the laser pulse maximum the differences begin to decrease and the curves become almost indistinguishable after $t - t_0 = 12$ ns. The transverse electron density distributions for different w_0 collapse approximately to a single density distribution around 12 ns after the heater maximum, see Fig. 11. In order to illustrate the effect of the laser heater on the transverse plasma density profile we show Fig. 12. The change of the plasma parameters due to the laser heater interaction with plasma take place in the central part of the capillary, for $r < 250$ μm. However, the actual heating occurs only for the region $r < 60$ μm. This is significantly smaller than the size of the plasma parameters disturbance due to laser heater. We conclude that the reason for the electron density aligning along the capillary axis is the fact that radial
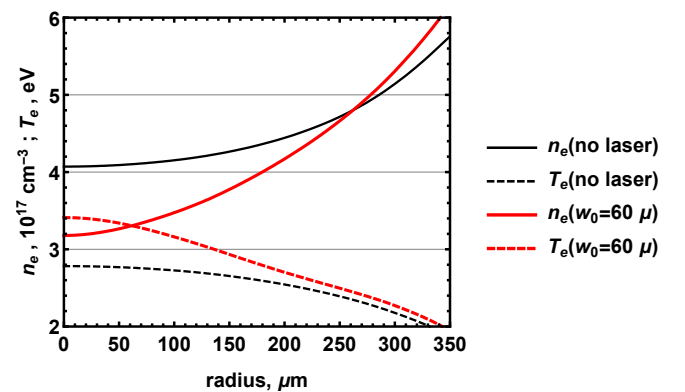
distributions of electron temperature and density in the laser assisted capillary discharge only weakly depend on the transverse size of the heater laser beam. The presented above results were obtained for $t_0 = 800$ ns. We also performed the 1D simulations for other t_0 that confirmed our main conclusion does not depend on t_0.

IV. CONCLUSIONS

In this paper we presented 2D simulations of the plasma dynamics in capillary discharges additionally heated by a laser pulse in order to create deeper and

more transversely confined plasma channels for subsequent high power laser guiding. The simulations show that a nearly axially uniform electron density profile is formed for some delay after the laser heater maximum. This effect contributed to the successful utilization of the laser-assisted capillary discharges in LWFA experiments yielding the record electron beam energy of 7.8 GeV [4, 19, 20].

We investigated the mechanism of the observed electron density axial uniformity, and showed that the uniformity is caused by the radial one-dimensional dynamics of the capillary discharge plasma and that it depends on the duration of the heater pulse. The axial uniformity of the plasma channel strongly depends on the delays between the electric current peak and the maximum of the laser heater, and between the maxima of the heater and of the high power femtosecond laser pulse. These simulations allow us to find optimal parameters to form axially uniform and deeper plasma channels for guiding high power laser with smaller spot sizes than would otherwise be possible in the discharge capillary.

DATA AVAILABILITY

The data that support the findings of this study are available from the corresponding author upon reasonable request.

[1] G. A. Mourou, T. Tajima, and S. V. Bulanov, Rev. Mod. Phys. **78**, 309 (2006).

[2] E. Esarey, C. B. Schroeder, and W. P. Leemans, Rev. Mod. Phys. **81**, 1229 (2009).

[3] S. M. Hooker, Nat. Photonics **7**, 775 (2013).

[4] A. J. Gonsalves, K. Nakamura, J. Daniels, C. Benedetti, C. Pieronek, T. de Raadt, S. Steinke, J. Bin, S. S. Bulanov, J. van Tilborg, C. G. R Geddes, C. B. Schroeder, Cs. Tóth, E. Esarey, K. Swanson, L. Fan-Chiang, G. Bagdasarov, N. Bobrova, V. Gasilov, G. Korn, P. Sasorov, and W. P. Leemans, Phys. Rev. Lett. **122**, 084801 (2019).

[5] W. P. Leemans, A. J. Gonsalves, H.-S. Mao, K. Nakamura, C. Benedetti, C. B. Schroeder, Cs. Tóth, J. Daniels, D. E. Mittelberger, S. S. Bulanov, J.-L. Vay, C. G. R. Geddes, and E. Esarey, Phys. Rev. Lett. **113**, 245002 (2014).

[6] N. A. Bobrova, A. A. Esaulov, J.-I. Sakai, P. V. Sasorov, D. J. Spence, A. Butler, S. M. Hooker, and S. V. Bulanov, Phys. Rev. E **65**, 016407 (2002).

[7] P. Sasorov, *"Plasma Dynamics in Capillary Discharges"*, in X-Ray Lasers 2016, Proceedings of the 15th Int. Conf. on X-Ray Lasers, (Eds. T. Kawachi, S. V. Bulanov, H. Daido, Y. Kato), Proceedings in Physics **202**, (Springer, 2018), p. 389.

[8] C. G. Durfee, and H. M. Milchberg, Phys. Rev. Lett. **71**, 2409 (1993).

[9] P. Volfbeyn and W. P. Leemans, in *Proceedings of the 6th European Particle Accelerator Conference*, edited by S. Myers, L. Liljeby, Ch. Petit-Jean-Genaz, J. Poole, and K. G. Rensfelt (Inst. of Phys., Philadelphia, 1998), p. 265.

[10] P. Volfbeyn, E. Esarey, and W. P. Leemans, Phys. Plasmas **6**, 2269 (1999).

[11] C. G. R. Geddes, Cs. Tóth, J. van Tilborg, E. Esarey, C. B. Schroeder, D. Bruhwiler, C. Nieter, J. Cary, and W. P. Leemans, Nature **131**, 538 (2004).

[12] C. G. R. Geddes, Cs. Tóth, J. van Tilborg, E. Esarey, C. B. Schroeder, J. Cary, and W. P. Leemans, Phys. Rev. Lett. **95**, 145002 (2005).

[13] A. Morozov, A. Goltsov, Q. Chen, M. Scully, and S. Suckewer, Phys. Plasmas **25**, 053110 (2018).

[14] R. J. Shalloo, C. Arran, A. Picksley, A. von Boetticher, L. Corner, J. Holloway, G. Hine, J. Jonnerby, H. M. Milchberg, C. Thornton, R. Walczak, and S. M. Hooker, Phys. Rev. Accel. Beams **22**, 041302 (2019).

[15] O. G. Olkhovskaya, G. A. Bagdasarov, N. A. Bobrova, V. A. Gasilov, L. V. N. Goncalves, C. Lazzarini, M. Nevrkla, G. Grittani, S. S. Bulanov, A. G. Gonsalves, C. B. Schroeder, E. Esarey, P. V. Sasorov, S. V. Bulanov, and G. Korn, J. Plasma Phys. **86**, 905860307 (2020).

[16] S. Steinke, J. van Tilborg, C. Benedetti, C. G. R. Geddes, C. B. Schroeder, J. Daniels, K. K. Swanson, A. J. Gonsalves, K. Nakamura, B. H. Shaw, E. Esarey, and W. P. Leemans, Nature **530**, 190 (2016).

[17] C. B. Schroeder, E. Esarey, C. G. R. Geddes, C. Benedetti, and W. P. Leemans, Phys. Rev. ST Accel. Beams **13**, 101301 (2010).

[18] N. A. Bobrova, P. V. Sasorov, C. Benedetti, S. S. Bulanov, C. G. R. Geddes, C. B. Schroeder, E. Esarey, and

W. P. Leemans, Phys. Plasmas **20**, 020703 (2013).

[19] A. J. Gonsalves, K. Nakamura, C. Benedetti, C. V. Pieronek, S. Steinke, J. H. Bin, S. S. Bulanov, J. van Tilborg, C. G. R. Geddes, C. B. Schroeder, J. Daniels, Cs. Tóth, L. Obst-Huebl, R. G. W. van den Berg, G. Bagdasarov, N. Bobrova, V. Gasilov, G. Korn, P. Sasorov, W. P. Leemans, E. Esarey, Phys. Plasmas **27**, 053102 (2020).

[20] C. Pieronek, A. Gonsalves, C. Benedetti, S. Bulanov, J. van Tilborg, J. Bin, K. Swanson, J. Daniels, G. Bagdasarov, N. Bobrova, V. Gasilov, G. Korn, P. Sasorov, C. Geddes, C. Schroeder, W. Leemans, and E. Esarey, Phys. Plasmas 27, 093101 (2020) (2020).

[21] J. van Tilborg, S. Steinke, C. G. R. Geddes, N. H. Matlis, B. H. Shaw, A. J. Gonsalves, J. V. Huijts, K. Nakamura, J. Daniels, C. B. Schroeder, C. Benedetti, E. Esarey, S. S. Bulanov, N. A. Bobrova, P. V. Sasorov, and W. P. Leemans, Phys. Rev. Lett. **115**, 184802 (2015).

[22] R. Pompili, M. P. Anania, M. Bellaveglia, A. Biagioni, S. Bini, F. Bisesto, E. Brentegani, G. Castorina, E. Chiadroni, A. Cianchi, M. Croia, D. Di Giovenale, M. Ferrario, F. Filippi, A. Giribono, V. Lollo, A. Marocchino, M. Marongiu, A. Mostacci, G. Di Pirro, S. Romeo, A. R. Rossi, J. Scifo, V. Shpakov, C. Vaccarezza, F. Villa, and A. Zigler, Appl. Phys. Lett. **110**, 104101 (2017).

[23] J. van Tilborg, S. K. Barber, H.-E. Tsai, K. K. Swanson, S. Steinke, C. G. R. Geddes, A. J. Gonsalves, C. B. Schroeder, E. Esarey, S. S. Bulanov, N. A. Bobrova, P. V. Sasorov, and W. P. Leemans, Phys. Rev. Accel. Beams **20**, 032803 (2017).

[24] R. Pompili, M. P. Anania, M. Bellaveglia, A. Biagioni, S. Bini, F. Bisesto, E. Brentegani, F. Cardelli, G. Castorina, E. Chiadroni, A. Cianchi, O. Coiro, G. Costa, M. Croia, D. Di Giovenale, M. Ferrario, F. Filippi, A. Giribono, V. Lollo, A. Marocchino, M. Marongiu, V. Martinelli, A. Mostacci, D. Pellegrini, L. Piersanti, G. Di Pirro, S. Romeo, A. R. Rossi, J. Scifo, V. Shpakov, A. Stella, C. Vaccarezza, F. Villa, and A. Zigler, Phys. Rev. Lett. **121**, 174801 (2018).

[25] C. A. Lindstrøm, E. Adli, G. Boyle, R. Corsini, A. E. Dyson, W. Farabolini, S. M. Hooker, M. Meisel, J. Osterhoff, J.-H. Röckemann, L. Schaper, and K. N. Sjobak, Phys. Rev. Lett. **121**, 194801 (2019).

[26] J.-H. Röckemann, L. Schaper, S. K. Barber, N. A. Bobrova, G. Boyle, S. S. Bulanov, N. Delbos, K. Floettmann, G. Kube, W. Lauth, W. P. Leemans, V. Libov, A. R. Maier, M. Meisel, P. Messner, P. V. Sasorov, C. B. Schroeder, J. van Tilborg, S. Wesch, and J. Osterhoff, Phys. Rev. AB **21**, 122801 (2018).

[27] E. Chiadroni, M. P. Anania, M. Bellaveglia, A. Biagioni, F. Bisesto, E. Brentegani, F. Cardelli, A. Cianchi, G. Costa, D. Di Giovenale, G. Di Pirro, M. Ferrario, F. Filippi, A. Gallo, A. Giribono, A. Marocchino, A. Mostacci, L. Piersanti, R. Pompili, J. B. Rosenzweig, A. R. Rossi, J. Scifo, V. Shpakov, C. Vaccarezza, F. Villa, A. Zigler, Nucl. Instrum. Methods Phys. Res., Sect. A **909**, 16, (2018).

[28] V. Gasilov, A. Boldarev, S. Dyachenko, O. Olkhovskaya, E. Kartasheva, G. Bagdasarov, S. Boldyrev, I. Gasilova, V. Shmyrov, S. Tkachenko, J. Grunenwald, and T. Maillard, *Applications, Tools and Techniques on the Road to Exascale Computing* (ed. by K. De Bosschere, E. H. D'Hollander, G. R. Joubert, D. Padua, and F. Peter), Advances in parallel computing, vol. **22**, (IOS Press; 2012) p. 235.

[29] C. Benedetti, C. B. Schroeder, C. G. R. Geddes, E. Esarey, and W. P. Leemans AIP Conference Proceedings **1299**, 250 (2010).

[30] C. Benedetti, C. B. Schroeder, C. G. Geddes, E. Esarey, and W. P. Leemans Plasma Phys. Control. Fusion **60**, 014002 (2018).

[31] S. I. Braginskii, Reviews of Plasma Physics, ed. by M. A. Leontovich, Consultants Bureau, New York, vol. 1 (1965).

[32] G. Bagdasarov, P. Sasorov, A. Boldarev, O. Olkhovskaya, V. Gasilov, A. Gonsalves, S. Barber, S. S. Bulanov, C. B. Schroeder, J. van Tilborg, E. Esarey, W. Leemans, T. Levato, D. Margarone, G. Korn, S. V. Bulanov, Physics of Plasmas **24**, 053111 (2017).

[33] G. Bagdasarov, P. Sasorov, V. Gasilov, A. Boldarev, O. Olkhovskaya, C. Benedetti, S. S. Bulanov, A. Gonsalves, H.-S. Mao, C. B. Schroeder, J. van Tilborg, E. Esarey, W. Leemans, T. Levato, D. Margarone, G. Korn, Physics of Plasmas **24**, 083109 (2017).

[34] G. Bagdasarov, N. Bobrova, A. Boldarev, O. Olkhovskaya, P. Sasorov, V. Gasilov, S. Barber, S. S. Bulanov, A. Gonsalves, C. B. Schroeder, J. van Tilborg, E. Esarey, W. Leemans, T. Levato, D. Margarone, G. Korn, M. Kando, S. V. Bulanov, Physics of Plasmas **24**, 123120 (2017).

[35] E. M. Lifshitz and L. P. Pitaevskii, *Physical Kinetics* (Pergamon Press, Oxford, 2002). [Sec. IV.48]

[36] I. I. Sobelman, *Atomic Spectra and Radiative Transitions*, (Springer, 1992, 2nd edition).

[37] N. A. Bobrova, S. V. Bulanov, T. L. Raznikova, and P V. Sasorov, Plasma Phys. Rep. **22**, 5 (1996).

[38] M. Vrbova, P. Vrba, A. Jancarek, M. Nevrkla, N. A. Bobrova, and P. V. Sasorov, Phys. Plasmas **26**, 083108 (2019).